Supplementary Information: Electric-Field-Triggered Ion Trapping for Non-Volatile Doping of Graphene Transistors

Dnyanesh D. Sarawate,[†] Priscilla M. Prem,[†] Eric J. Beckman,[†] Ke Xu,[*,‡,¶] and Susan K. Fullerton-Shirey[*,†,§]

[†]*Department of Chemical and Petroleum Engineering, University of Pittsburgh, Pittsburgh, PA*

[‡]*Department of Physics and Astronomy, Rochester Institute of Technology, Rochester, NY*

[¶]*Microsystems Engineering, Rochester Institute of Technology, Rochester, NY*

[§]*Department of Electrical and Computer Engineering, University of Pittsburgh, Pittsburgh, PA*

E-mail: ke.xu@rit.edu; fullerton@pitt.edu

Part 1: Ion mobility and EDL dynamics of poly(DEAEMA-co-PEGMA) electrolytes

The temperature-dependent ionic conductivity of poly(DEAEMA-co-PEGMA) and $LiClO_4$ is reported in the main manuscript, Figure 1c, with a molar ether oxygen to Li^+ ratio of 20:1 . Here, the raw impedance and phase angle data, along with the calculated frequency-dependent conductivity are show in Figure S1. The DC conductivity in Figure 1c corresponds to the frequency-independent conductivity in Figure S1(c) and (f).

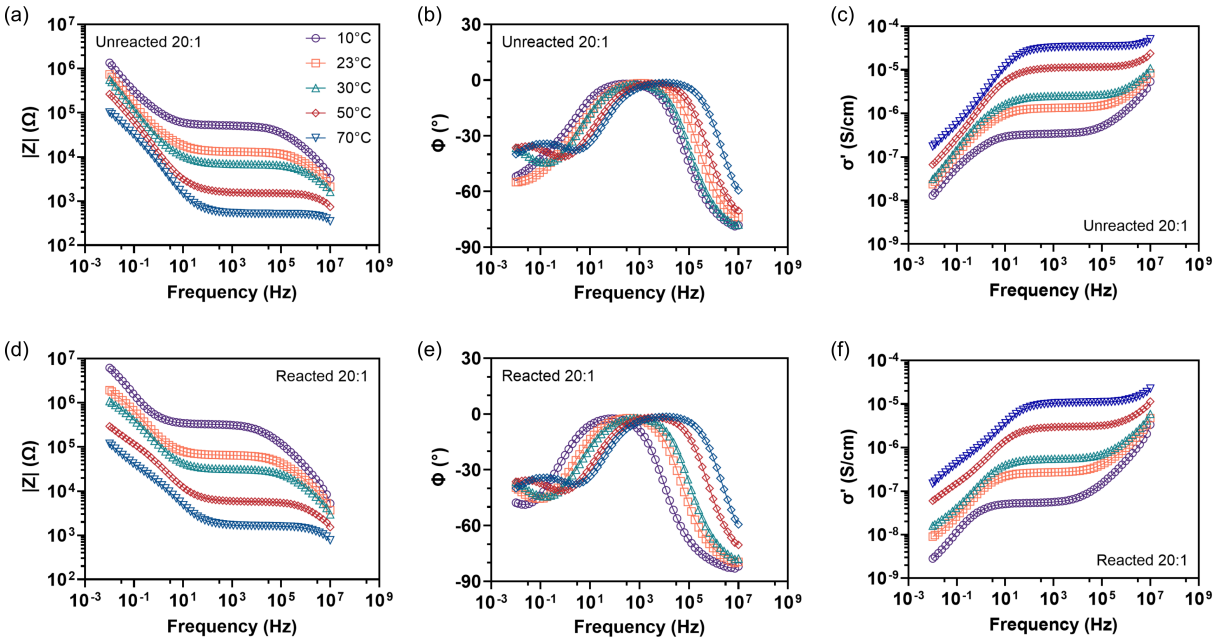

Figure S1: **Impedance data** Frequency-dependent (a, d) impedance, (b, e) phase angle and (c, f) conductivity of poly(pDEA-co-PEGMA) and $LiClO_4$ with EO:Li^+ = 20:1 before (top row) and after (bottom row) thermal crosslinking at 70 °C for 24 hours.

Impedance measurements quantify bulk ion mobility, and time-dependent current-voltage (IV) measurements capture EDL dynamics. Lateral Ti/Au (5/145 nm) capacitors were defined on 90 nm SiO_2/Si using a maskless aligner (Heidelberg MLA100 Direct Write Lithographer). Figure S2(a) is an optical image of a lateral capacitor with an electrode separation distance of 5 μm. Lateral capacitors were chosen because of the easy fabrication process and straightforward measurement (i.e., the signature of ion mobility is a time-dependent current

response to a voltage on the timescale of milliseconds to seconds.

Poly(DEAEMA-co-PEGMA) with and without salt and crosslinker were deposited on the capacitors by drop-casting 25 μL of 1 wt% electrolyte in acetonitrile. Figure S2 (b) are the time-dependent IV (IV-t) measurements comparing the neat co-polymer, co-polymer with salt (EO:Li^+ molar ratio of 350:1), co-polymer with DBH crosslinker (DEAEMA:DBH molar ratio of 2:1), and co-polymer with salt and crosslinker.

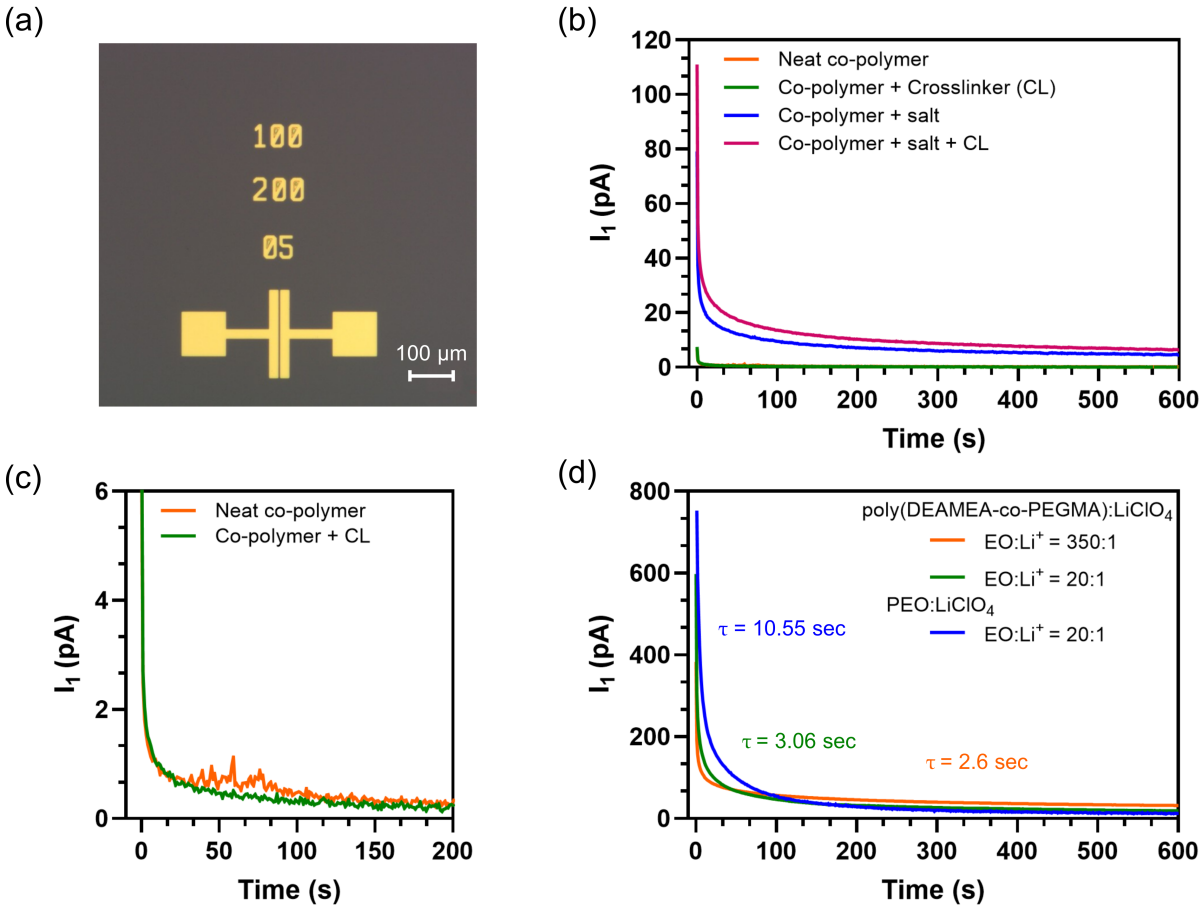

Figure S2: **Electrical conductivity (a)** Optical image of a lateral capacitor with 5 μm distance between the plates. **(b)** IV-t of poly(DEAEMA-co-PEGMA) neat polymer, with salt (EO:Li^+ = 350:1), with crosslinker (CL) added (no salt), and with salt and crosslinker. **(c)** IV-t from (b) of poly(DEAEMA-co-PEGMA) neat polymer and with crosslinker only zoomed in on y-axis at low current. **(d)** IV-t of poly(DEAEMA-co-PEGMA)(EO:Li^+ = 350:1 and 20:1) and polyethylene oxide (PEO) (EO:Li^+ = 20:1). For all measurements V_1 = 3 V, V_1 = 0 V and T = 296 K.

In the polymer without salt and crosslinker, only a dissipation current of $< 10\ pA$ is

observed (see Figure S2 (c)). In samples containing ions, EDL formation is detected as a larger initial current ($> 60\ pA$) followed by current saturation as the EDL approaches its fully formed state and ion mobility decreases. The initial charging current is the largest ($\sim$110 pA) when both the crosslinker and salt are included, suggesting that the crosslinker favors EDL formation.

Figure S2 (d) shows the impact of salt concentration and polymer identity on EDL formation dynamics. PEO:$LiClO_4$ with a molar ratio of 20:1 is included because it is frequently used to gate 2D FETs[1,2] and this particular concentration is known to give the largest ion mobility in PEO:$LiClO_4$.[3] To quantify the formation time, the data are fit to a stretched exponential:[4]

$$\frac{I_1}{I_0} = (1 - E) \exp\left(-\left(\frac{t}{\tau}\right)^{\beta}\right) + E \tag{1}$$

where I_1 is the measured current, I_0 is the current at the first time point, E is a fraction of current that decays outside the time window of the measurement, τ is the time constant, and β is a stretching factor ranging from 0.2 to 0.5, indicating the distribution of time constants. All time constants are on the order of seconds, confirming that the charging current is due to ion mobility and not electron/hole transport.

Part 2: AFM Cleaning

AFM contact-mode cleaning is use to remove lithography residue from the channel surface to maximize the ionic gate control.[5] Topographical AFM scans of the channel of device D2 before and after cleaning are provided in Figure S3 (a) and (b), respectively. Each scan is 256 lines. Figure S3 (c) show step height scans corresponding to the locations at the edge of the flake shown by the white rectangle in (a) and (b). The flake is ≈1.1 nm thick and the polymer residue is approximately 0.8 nm thick. Transfer measurements before and after cleaning are shown in Figure S3 (d). The Dirac point shifts from +2 to -1 V after cleaning, indicating that the lithographic polymer residue induced some p-type doping.

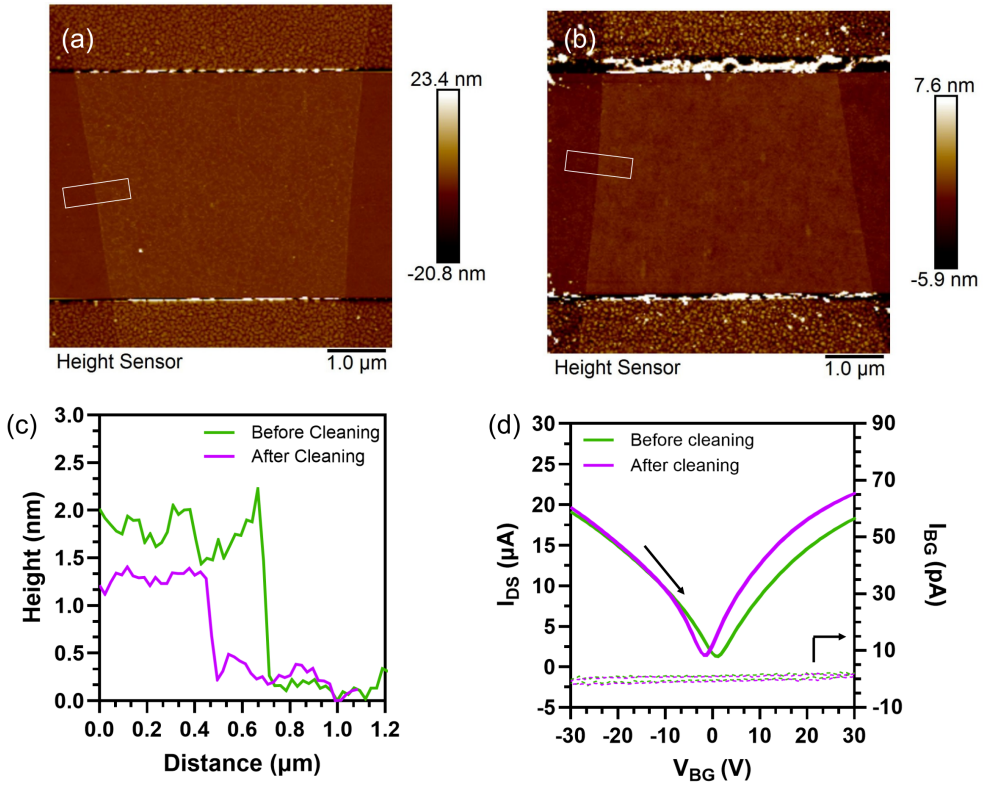

Figure S3: **AFM cleaning of lithographically patterned FET.** Topography AFM scan of the channel of device D2 **(a)** before and **(b)** after cleaning. **(c)** Step height scans corresponding to the locations indicated by the white rectangles in (a) and (b). **(d)** Transfer characteristics before and after cleaning of device D2 with $V_{DS} = 10\ mV$, T = 296 K, Sweep rate ≈ 6.3 V/s

Part 3: Side-gated measurements

Double-sweep transfer characteristics in Figure S4(a) show both sweeps for device D1 (the data in Figure 2c of the main text includes only the initial, single sweep). The hysteresis between the forward and reverse sweeps highlights the sluggish ionic dynamics.

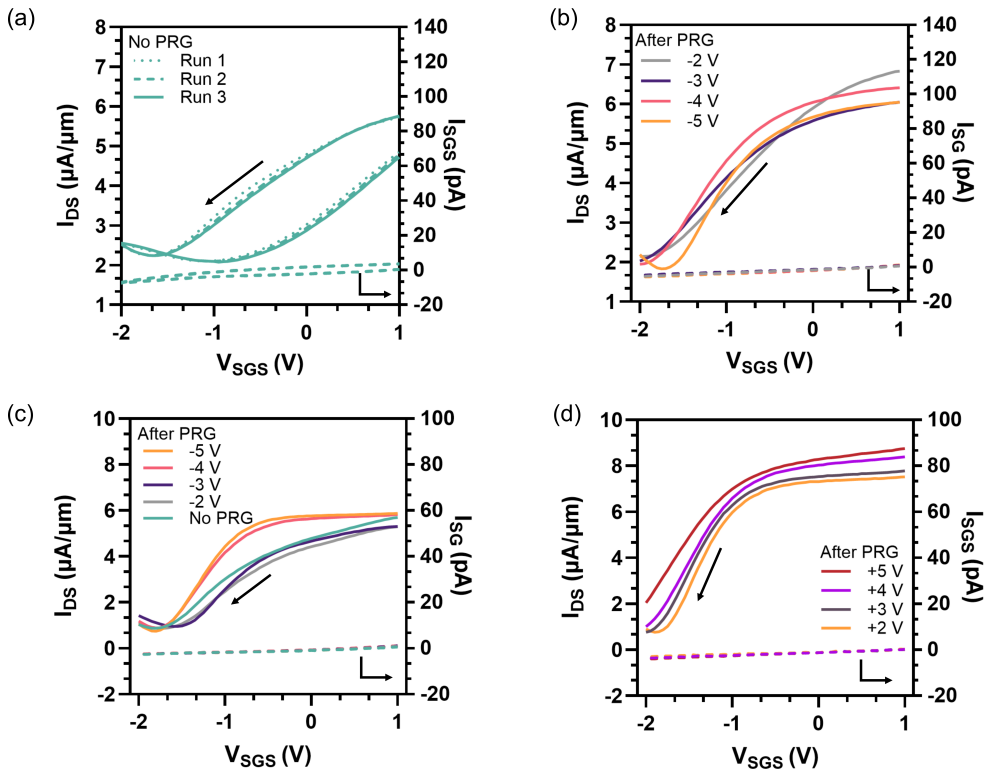

Figure S4: **Side-gated transfer measurements (a)** Three consecutive double-sweep measurements of device D1 before programming. **(b)** Initial sweep ($+V_{SGS}$ to $-V_{SGS}$) of device D1 programmed sequentially with increasingly negative programming bias after the positive programming sequence was completed in Figure 2 (d) of the main manuscript. $V_{DS} = 20\ mV$, T = 310 K, Sweep rate = 1 mV/s, EO:Li^+ = 350:1. Transfer characteristics of Device D2 **(c)** when unprogrammed and then programmed sequentially at increasing negative gate bias, and **(d)** programmed sequentially at increasing positive gate bias after negative programming in (c). $V_{DS} = 10\ mV$, T = 296 K, Sweep rate = 1 mV/s, EO:Li^+ = 350:1.

Figure S4(b-d) show initial, single-sweep transfer data for devices D1 and D2 under varying programming sequences. Figure S4(b) corresponds to device D1, showing the complete set of transfer curves for negative programming steps, extending the data shown in the main manuscript in Figure 2(d). Figure S4(c) and SS4(d) correspond to device D2, where the

programming sequence was reversed from that of D1 (i.e., negative programming followed by positive programming).

Part 4: Dirac point shift due to temperature

Measurements of the glass transition temperature (T_g) in Figure 1c of the main manuscript do not provide a clear indication of the onset of polymer mobility. This is not unusual given the temperature range of most DSC instruments and the fact that T_g is a broad, second-order phase transition. To confirm the onset of ion mobility in a FET, the device was cooled to 153 K, which is well below the midpoint T_g detected by DSC, and heated in 10 K increments to nearly 400 K. Transfer characteristics (I_D–V_{SGS}) were measured at each temperature to monitor the onset of gate modulation.

As shown in Figure S5(a) and (b), no gate modulation is observed until 233 K, at which point a clear modulation in I_{DS} with V_{SGS} was detected. At temperatures above the T_g (273 K and 283 K), the modulation increases significantly. The degree of modulation was quantified by the ON/OFF ratio and hysteresis (difference in V_{SGS} required to achieve the same I_{DS} in forward and reverse sweeps). The highest ON/OFF ratio and minimum hysteresis were observed after heating to 303 K, which is expected, as it is about 60 °C above the T_g.

Another observation from the thermal experiments was the gradual shift in the graphene Dirac point after multiple heat–cool–heat cycles, even in the absence of an applied programming voltage. Notably, the repeatable transfer measurements of Figure S4(a) confirm that no significant polymer crosslinking occurs at room temperature, suggesting that the observed shift with temperature is not caused by chemical changes.

Interestingly, the Dirac point shift stabilizes once the device undergoes a complete thermal conditioning cycle: heating to 300 K, cooling to 200 K, then reheating to 300 K followed by isothermal hold for approximately 12 hours. After this process, no further drift in the Dirac point is observed under ambient conditions. This behavior implies that the initial shifts are

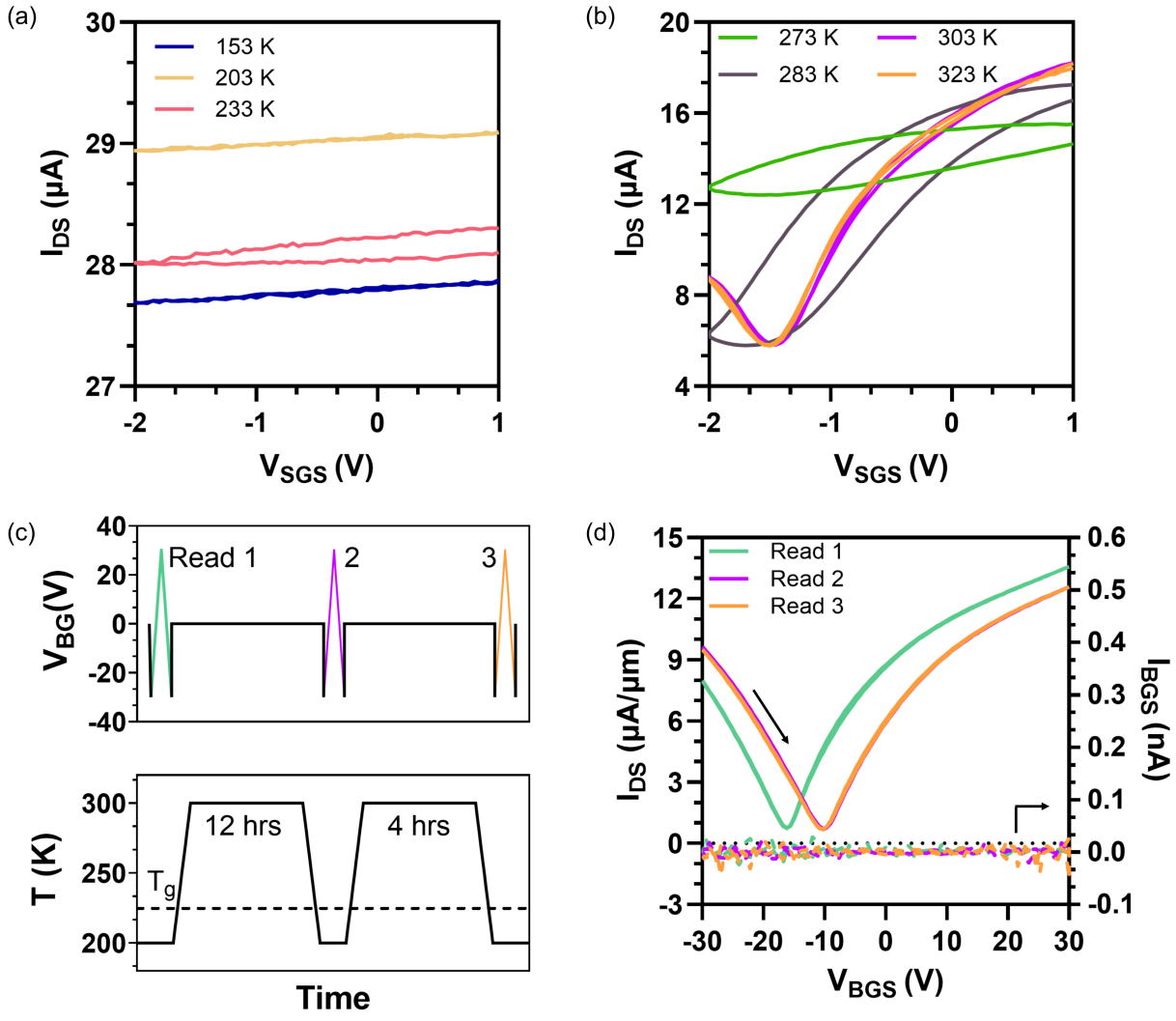

Figure S5: **Thermal response of poly(pDEA-co-PEGMA)** Drain current(I_{DS}) modulation with increasing temperature from **(a)** 153 to 233 K and **(b)** 273 to 323 K with V_{DS} = 10 mV, Sweep rate = 10 mV/s, EO:Li^+ = 350:1. **(c)** Initial thermal sequence to stabilize the Dirac point. **(d)** Transfer characteristics of device D5 before and after following the thermal protocol in (c) with V_{DS} = 10 mV, T = 200 K, Sweep rate ≈ 3-7 V/s, EO:Li^+ = 20:1.

likely related to thermomechanical effects within the polymer rather than electrochemical programming. Although we cannot know for sure, the Dirac point shift could possibly arise from thermally induced changes in strain, which can impact graphene doping.[6] When the polymer is drop-cast on graphene, it changes in morphology during temperature cycling likely alter the local interfacial structure, and could shift the Fermi level of the graphene.[7–9]

Once the polymer is stabilized with thermal cycling and annealing, the Dirac point is no longer temperature-sensitive.

The stabilization procedure is illustrated in Figure S5(c), where the programming sequence used to condition the device is shown. Transfer characteristics corresponding to Figure S5(c) are presented in Figure S5(d). This procedure is carried out before any programming sequences are preformed to ensure that any subsequent Dirac point shift is due to intentional programming rather than unintentional thermal–mechanical effects.

Part 4: Control measurements

Control measurements in Figure S6 confirm that the observed Dirac point shift originates from the programming of the crosslinked polymer electrolyte, and verify the proposed mechanism of ion trapping in the EDL. The polymer electrolyte was prepared without crosslinker, leaving only the polymer matrix with dissolved ions in a concentration of EO:Li^+ = 350:1. This formulation lacks the ability to undergo crosslinking, and, therefore, cannot trap ions in the EDL upon e-field programming. The control electrolyte was drop-cast onto a fresh graphene FET, device D9, under identical conditions as the FETs with crosslinkers to ensure consistent interfacial behavior and comparable initial doping levels.

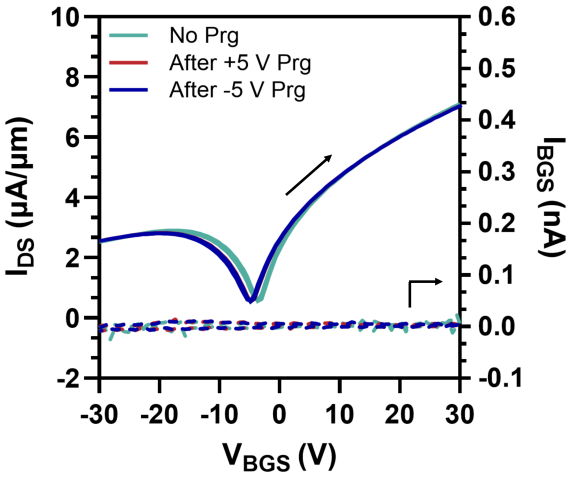

Figure S6: **Transfer characteristics of control devices before and after programming.** Transfer characteristics of device D9: poly(DEAEMA-co-PEGMA) with EO:Li^+ = 350:1 and no crosslinker. $V_{DS} = 10\ mV$, T = 200 K, and Sweep rate ≈ 6.3 V/s.

The same programming sequence that was applied in Figure 4(a) of the main manuscript was used for the control device. The resulting transfer characteristics in Figure S6 show no significant Dirac point shift on programming. Thus, the non-volatile Dirac point shift shown in Figure 4 of the main manuscript occurs only when the crosslinker is included, supporting the proposed mechanism of ion immobilization within the crosslinked polymer.

References

(1) Kim, S. H.; Hong, K.; Xie, W.; Lee, K. H.; Zhang, S.; Lodge, T. P.; Frisbie, C. D. Electrolyte-gated transistors for organic and printed electronics. 2013.

(2) Li, H. M.; Xu, K.; Bourdon, B.; Lu, H.; Lin, Y. C.; Robinson, J. A.; Seabaugh, A. C.; Fullerton-Shirey, S. K. Electric Double Layer Dynamics in Poly(ethylene oxide) LiClO4 on Graphene Transistors. *Journal of Physical Chemistry C* **2017**, *121*, 16996–17004.

(3) Fullerton-Shirey, S. K.; Maranas, J. K. Effect of LiClO 4 on the structure and mobility of PEO-based solid polymer electrolytes. *Macromolecules* **2009**, *42*, 2142–2156.

(4) Lukichev, A. Physical meaning of the stretched exponential Kohlrausch function. *Physics Letters, Section A: General, Atomic and Solid State Physics* **2019**, *383*, 2983–2987.

(5) Liang, J.; Xu, K.; Toncini, B.; Bersch, B.; Jariwala, B.; Lin, Y. C.; Robinson, J.; Fullerton-Shirey, S. K. Impact of Post-Lithography Polymer Residue on the Electrical Characteristics of MoS 2 and WSe 2 Field Effect Transistors. *Advanced Materials Interfaces* **2019**, *6*.

(6) Sharifzadeh, E.; Cheraghi, K. Temperature-affected mechanical properties of polymer nanocomposites from glassy-state to glass transition temperature. *Mechanics of Materials* **2021**, *160*, 103990.

(7) Levesque, P. L.; Sabri, S. S.; Aguirre, C. M.; Guillemette, J.; Siaj, M.; Desjardins, P.; Szkopek, T.; Martel, R. Probing charge transfer at surfaces using graphene transistors. *Nano Letters* **2011**, *11*, 132–137.

(8) Wu, G.; Tang, X.; Meyyappan, M.; Lai, K. W. C. Doping effects of surface functionalization on graphene with aromatic molecule and organic solvents. *Applied Surface Science* **2017**, *425*, 713–721.

(9) Wang, L.; Sofer, Z.; Pumera, M. Will Any Crap We Put into Graphene Increase Its Electrocatalytic Effect? *ACS Nano* **2020**, *14*, 21–25.